Integrative Biology

Accepted Manuscript

ROYAL SOCIETY OF CHEMISTRY

www.rsc.org/ibiology

ARTICLE TYPE www. rsc.org/xxxxxx | XXXXXXXX

Modulation of T-cell receptor functional sensitivity via the opposing actions of protein tyrosine kinases and phosphatases: a mathematical model

Barbara Szomolay[a] **and Hugo A. van den Berg**[*a]

Received Xth XXXXXXXXXX 20XX, Accepted Xth XXXXXXXXX 20XX
First published on the web Xth XXXXXXXXXX 200X
DOI: 10.1039/b000000x

Combining receptor kinetics and stochastic modelling of receptor activation, we show that a T-cell can specifically augment its functional sensitivity to one particular peptide ligand while simultaneously decreasing its sensitivity to other ligands, by coordinating the expression levels of the co-receptor CD8 and the relative activities of kinases and phosphatases in the vicinity of the T-cell receptor (TCR). We propose that this focusable degeneracy of epitope recognition allows a TCR to have a wide range of potential ligands but be specifically sensitive to only one or a few of these at any one time, which resolves the paradox of how a relatively small number of clones ($\sim 10^6$) can maintain the potential to respond to a vast space of ligands ($\sim 20^9$) whilst avoiding auto-immunity. We validate the model against experimental data and predict shifts in functional sensitivity following a shift in the kinase/phosphatase balance (which could in principle be induced by experimental means). Moreover, we propose that *in vivo*, the T-cell gauges ligand quality by monitoring changes in TCR triggering rate concomitant with shifts in this balance, for instance as the immunological synapse matures.

Insight, innovation, integration

Insight: TCR degeneracy is a dynamic quantity; modulation of the triggering threshold of the T-cell receptor is key to resolving the degeneracy paradox surrounding the T-cell repertoire. *Innovation*: Predictions are made regarding differential shifts in functional sensitivity in proposed phosphatase knock-down experiments. *Integration*: Properties at the level of the whole organism are explained in terms of molecular-cellular characteristics. Furthermore, the quantitative model predicts how manipulation of co-receptor and phosphatase levels will affect cross-reactivity and specificity at the whole-repertoire level.

1 Introduction

T-cell immunity relies on antigen recognition by the T-cell receptor (TCR)[1–3]. When the TCR engages a peptide ligand bound to a Class I peptide-major histocompatibility complex molecule (pMHCI), it transmits signals via the associated CD3 complex to the cellular interior where a variety of cellular responses can ensue[4]. The interactions with pMHCI ligands can loosely be classed as "weak" and "strong," the latter being typical of interactions underlying the recognition of pathogens, whereas weak interactions predominate in the case of peptides derived from the host's own proteome[1]. Such self recognition is a double-edged sword, since it is essential to both the formation and the maintenance of a diverse TCR repertoire containing $\sim 2.5 \times 10^8$ different TCRs[5,6], but can also lead to autoimmune disease[7]. TCR/pMHCI recognition is highly specific; the chances that a given pMHCI ligand will act as a strong agonist for a TCR picked at random have been estimated[8] to lie in the range 10^{-5}–10^{-7}. Yet a considerable degree of degeneracy remains: a single TCR may be able to engage in physiologically significant interactions with $\sim 10^6$ different peptides[7].

The CD3 complex consists of the CD3$\gamma\varepsilon$ and CD3$\delta\varepsilon$ heterodimers and the CD3$\zeta\zeta$ homodimer[9]. Following TCR/pMHCI ligation, lymphocyte-specific protein tyrosine kinase (Lck) phosphorylates the immuno-receptor tyrosine-based activation motifs (ITAMs), three of which are located on each ζ-chain and one of which is present in each of the other four peptide chains of the CD3 complex[9]. The phosphorylated ITAMs subsequently recruit protein kinases, such as ZAP70, and scaffold proteins, such as the linker for activation of T-cells, which mediate the initiation of intracellular signalling cascades[2].

The TCR/CD3 complex usually operates in concert

[a] *University of Warwick, Coventry CV4 7AL, United Kingdom; E-mail: hugo@maths.warwick.ac.uk*

with a co-receptor, which is CD8 for MHCI-restricted TCRs and which is thought to assist in the weak-type interactions[10], via several modes of action, such as enhancement of TCR/pMHCI stability[11,12] and delivery of Lck to TCR/CD3[13]. These effects tend to (i) prolong the average duration of a TCR/pMHCI contact and (ii) reduce the time required for the ITAMs to become phosphorylated and trigger intracellular signalling, both of which can enhance efficacy of weak ligands but which may equally well reduce that of strong ligands[14]. Since CD8 modulates the relative strength of peptide agonists, it has been proposed that T-cells vary CD8 levels to fine-tune their antigen sensitivity and general level of degeneracy in order to strike a balance between the need for strong responsiveness to salient ligands and sufficiently weak responsiveness to self-derived peptides[12,14].

The quality of the interaction between a given TCR and a given pMHCI ligand is experimentally quantified by means of a peptide titration assay[1]; this yields an empirical measure of agonist strength known as the functional sensitivity. Under suitable assumptions, this empirical measure can be taken to correspond to the rate at which a single pMHCI is able to elicit TCR triggering events, called the TCR triggering rate[8,15,16]. The TCR triggering rate is believed to depend primarily on the average TCR/pMHCI dwell-time (which is the reciprocal of the dissociation rate)[17,18], although the affinity of the TCR/pMHCI interaction (the ratio of dissociation rate and association rate) has also been proposed as the dominant factor[3,19]. Kinetic analysis reveals that both parameters play a role, their relative importance depending on the surface densities of TCR and pMHCI molecules[4,8].

The rate at which the TCR/CD3 complex transits through the ITAM phosphorylation sequence depends on the relative concentrations of protein tyrosine kinases (PTKs) and protein tyrosine phosphatases (PTPs) in the vicinity of the TCR/CD3 complex; these PTPs may be associated with receptors (such as CD45 and CD148) or cytoplasmic factors (such as SHP-1, PTPN3, PTPN4, and PTPN22)[20,21]. The PTP CD45 is a highly abundant PTP[22], which acts to de-phosophorylate ITAMs, counteracting the effect of Lck[23]. This PTP also dephosphorylates both the activating tyrosine residue of Lck (Tyr394) and the inhibitory residue of Lck (Tyr505), but affects the former more strongly, thus having a net inhibitory effect[20,21]. In addition, a plethora of positive (*i.e.*, CD28) and negative (*i.e.*, KIR) regulators in T-cells influence the PTK/PTP balance[24].

In the present paper, we generalise the kinetic proofreading model[25] by allowing not only ITAM phosphorylarion events, but de-phosphorylation events as well. Furthermore, we investigate the modulatory role of the co-receptor CD8 in a kinetic model of the interactions between TCR, pMHCI, and CD8. We show that the PTK/PTP balance modulates functional sensitivity and degeneracy by regulating the average time required for a TCR/CD3 complex to become triggered. This balance can evolve over the duration of a single interaction between a T-cell and an antigen-presenting cell (APC)[21,26–28], and also over the lifetime of the T-cell as it goes through various stages of differentiation[29], which indicates that TCR degeneracy should itself be regarded as a dynamic quantity that can be independently regulated for different clones or even for different T-cells within a given clone.

2 Theory

Receptor-ligand engagement initiates a sequence of events that include covalent modifications of the intracellular domain of the receptor, such as phosphorylation of ITAM tyrosine residues by PTKs, as well as molecular aggregation events (docking of further kinases and linkers for signalling). The essential idea of the kinetic proofreading model[25] is that this constitutes a sequence of states, which in the simplest version of the theory can be arranged in a linear sequence with the "resting" TCR/CD3 at one extreme and the fully modified TCR/CD3, now called the signalosome, at the other. The natural mathematical representation of such a system is a continuous-time Markov chain, as shown in Fig. 1.

If only "forward" steps are considered, we can immediately deduce that the average time required to attain the final state, also called the triggered state, is the sum of the average waiting times for the individual forward steps. Moreover, as the number of steps increases, the probability mass becomes concentrated on this average, which effectively acts as a threshold time: TCR/pMHCI dockings lasting longer than this time are almost certain to attain the triggered state, and for shorter-lasting dockings, triggering is almost certain not to occur. In Fig. 1, the forward rate has been taken as $n\lambda$, where n is the number of steps; the average time to triggering is thus λ^{-1}, which is the sharp triggering threshold when the backward rate is zero ($\psi = 0$).

The novel element in this study is the inclusion of "backward" steps that correspond to de-phosphorylation of ITAMs by PTPs. Intuitively, we expect this modification to prolong the average time to achieve triggering, and cause the probability mass to become less concentrated, that is, the threshold to become less sharp.

In addition to these Markov models of TCR/CD3 triggering, we calculate the densities of four possible coordinated states of the pMHCI molecule using kinetic equi-

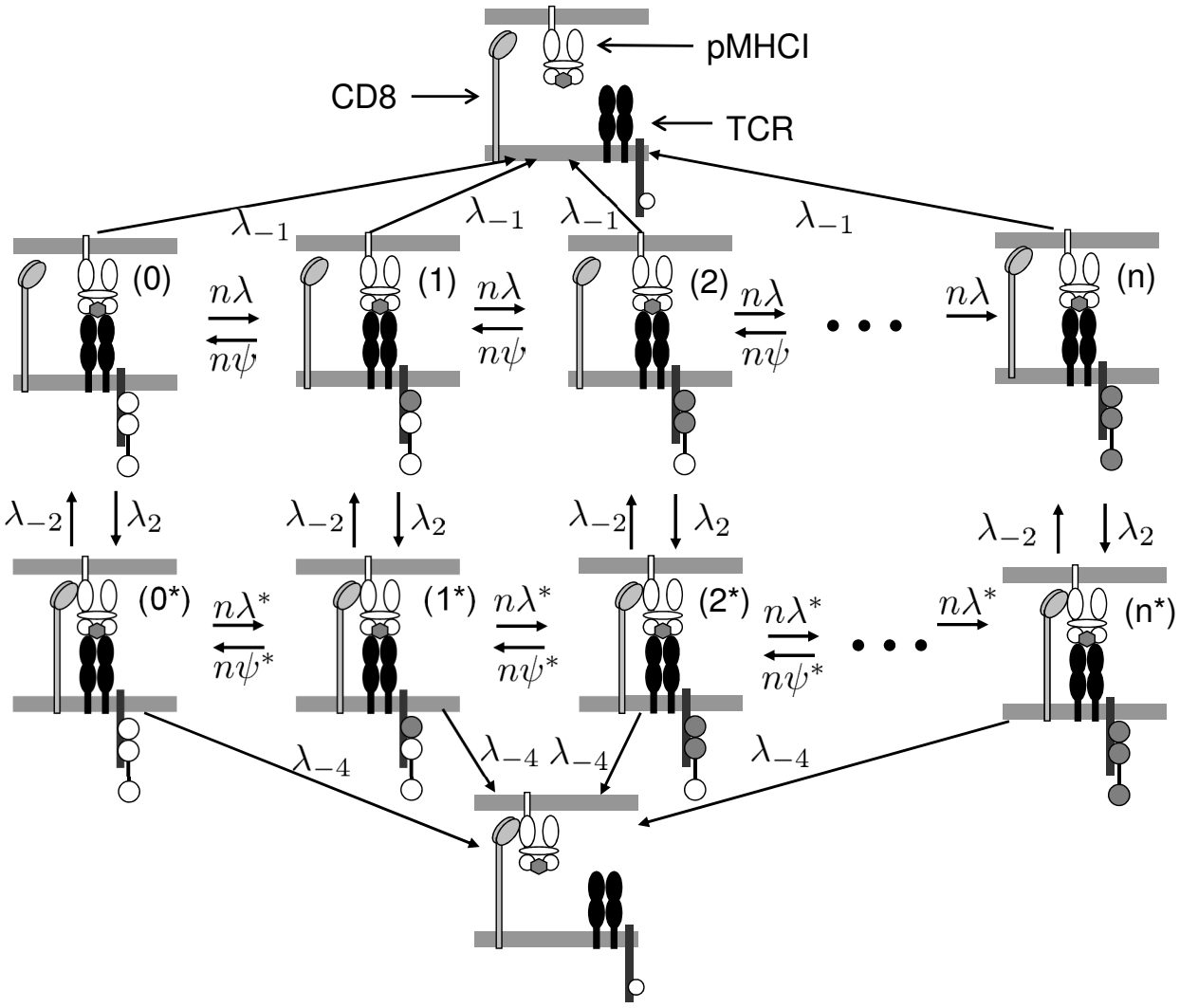

Fig. 1 Markov chain representation of the ITAM phosphorylation sequence in the TCR/CD3 complex The two horizontal chains both depict a linear sequence in which the ITAMs associated with the cytoplasmic tails of the CD3 complex become successively phosphorylated. The ITAMs are depicted as circles, which are initially all open to suggest the unphosphorylated state and eventually are all closed to suggest full phosphorylation. There are two chains which differ according to whether or not the co-receptor CD8 is bound to the pMHCI complex; λ_2 and λ_{-2} are the association and dissociation rates, respectively. The rates of the two main chains are affected by binding of CD8; when CD8 is not bound, forward steps proceed at a rate $n\lambda$, where n is the number of steps (ITAMs to be phosphorylated) and backward steps at a rate $n\psi$ (this scaling ensures that the unidirectional mean transversal times for the chains are λ^{-1} and ψ^{-1}, respectively, regardless of n). When CD8 is bound, these rates are $n\lambda^*$ and $n\psi^*$, respectively. Also indicated are TCR/pMHCI dissociation events, which happen at rate λ_{-1} when CD8 is not bound and at rate λ_{-4} when CD8 is bound. In the present development of the model, these events are assumed to result in a very rapid "reset" of the ITAM phosphorylation state to zero (all unphosphorylated). The final (triggered) states (n) and (n^*) are absorbing, that is, the TCR/CD3 signalling machinery is assumed to "click" into signalosome status.

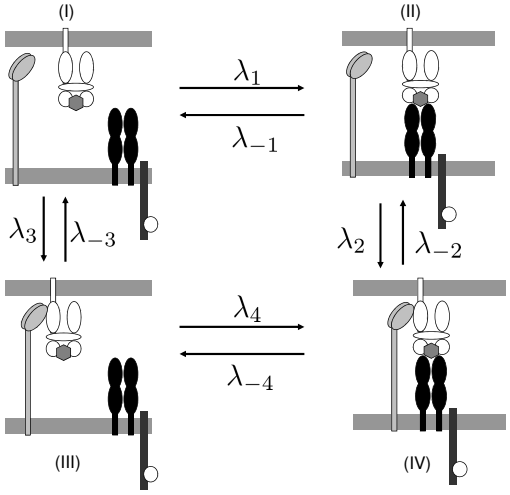

Fig. 2 Four states of coordination for the pMHCI molecule (I) free pMHCI; (II) pMHCI bound to TCR but not CD8; (III) pMHCI bound to CD8 but not TCR; (IV) pMHCI bound to both TCR and CD8. Rates are labeled as λ_i or λ_{-i} as indicated, where $i \in \{1,2,3,4\}$. The white circles in the cytoplasmic tails of the TCR/CD3 complex represent the ITAMs. For clarity, only one such tail and a single ITAM is indicated (the model more generally presupposes that there are n ITAMs).

librium (Fig. 2). These four states are: (I) free pMHCI; (II) pMHCI bound to TCR but not CD8; (III) pMHCI bound to CD8 but not TCR; (IV) pMHCI bound to both TCR and CD8. These states are represented by the corresponding Roman numerals in Fig. 2. The Markov states form a subdivision of states II and IV. It should be emphasised that whereas kinetic equilibrium is assumed to calculate the partitioning over states I–IV, the Markov chain restarts whenever the TCR engages a pMHCI; this chain is used to calculate the probability that the TCR/CD3 complex has been triggered when a given TCR/pMHCI docking terminates. We assume for the sake of simplicity that the receptor reverts to its basal state and no TCR signalling occurs if the ligand dissociates before the series of modifications is complete. The kinetic theory was presented earlier[30,31] and is briefly recapitulated in Appendix A to render the present paper self-contained. (The results that follow can, in principle, be obtained by continuous-time Monte Carlo simulations[32] and averaging a sufficiently large number of runs, but more efficient methods will be used.)

2.1 TCR triggering

ITAM phosphorylation events proceed at a rate $n\lambda$ when the co-receptor is not bound to the TCR/pMHCI complex, and at a rate $n\lambda^*$, when the co-receptor CD8 is bound, as shown in Fig. 1. Similarly, ITAM dephosphorylation events, corresponding to the backward arrows, proceed at rates $n\psi$ and $n\psi^*$ according as to whether CD8 is bound. (The inclusion of the parameter n in these rates is merely a matter of convenient scaling.)

The pMHCI/TCR docking may terminate before the triggered state (n) is reached. The pertinent dissociation rates are λ_{-1} for CD8-unbound and λ_{-4} for CD8-bound (we have $\lambda_{-4} \leq \lambda_{-1}$[14]). We assume that the unengaged TCR/CD3 complex is susceptible to very rapid dephosphorylation, so that it has virtually always reverted to the basal state (0) by the time it engages next with a pMHCI ligand. Thus, we assume that the system in states I and III (Fig. 2) only occurs with zero phosphorylated ITAMs (*i.e.*, the "resetting" to the basal state is quasi-instantaneous).

The rate at which TCR/CD3 complexes are triggered can be calculated as the rate at which TCR/pMHCI dissociations take place, weighted by the probability that the sequence of ITAM phosphorylations was complete at the point of break-up. In formula:

$$W = \lambda_{-1} M_R \mathbb{P}_0^0 + \lambda_{-4} M_{XR} \mathbb{P}_0^* \tag{1}$$

where M_R is the surface density of TCR/pMHCI complexes (with no CD8 bound) and M_{XR} is the surface density of TCR/pMHCI/CD8 complexes (see Appendix A for more details), and $\mathbb{P}_0^0$ denotes the probability that a TCR/CD3, starting from state (0), will attain the final state before TCR/pMHCI break-up, and, similarly, $\mathbb{P}_0^*$ denotes the probability that a TCR/CD3, starting from state (0^*), will attain the final state before TCR/pMHCI break-up. The kinetics calculation yields M_X and M_{XR}, so all that remains to be done is to calculate the probabilities $\mathbb{P}_0^0$ and $\mathbb{P}_0^*$.

The probability that the TCR/CD3 complex will undergo ITAM phosphorylation is given by

$$\mathbb{P}_a^0 = \frac{n\lambda}{\lambda_{-1} + n\lambda + n\psi + \lambda_2} \tag{2}$$

when the co-receptor CD8 is not engaged, and

$$\mathbb{P}_a^* = \frac{n\lambda^*}{\lambda_{-2} + n\lambda^* + n\psi^* + \lambda_{-4}} \tag{3}$$

when CD8 is engaged. Similarly, the probability that the TCR/CD3 complex will undergo ITAM dephosphorylation is given by

$$\mathbb{P}_b^0 = \frac{n\psi}{\lambda_{-1} + n\lambda + n\psi + \lambda_2} \tag{4}$$

when CD8 is not engaged, and

$$\mathbb{P}_b^* = \frac{n\psi^*}{\lambda_{-2} + n\lambda^* + n\psi^* + \lambda_{-4}} \tag{5}$$

when CD8 is engaged. Finally, the probability that the system switches from the chain with CD8 unengaged to the chain with CD8 engaged is given by

$$\mathbb{P}_c^0 = \frac{\lambda_2}{\lambda_{-1} + n\lambda + n\psi + \lambda_2} \tag{6}$$

whereas the probability that the system switches from the chain with CD8 engaged to the chain with CD8 unengaged is given by

$$\mathbb{P}_c^* = \frac{\lambda_{-2}}{\lambda_{-2} + n\lambda^* + n\psi^* + \lambda_{-4}} \,. \tag{7}$$

TCR triggering requires the completion of all ITAM phosphorylation steps before the TCR/pMHCI complex disassociates. Hence, we consider the probability that the TCR/CD3 complex will attain the final state, either (n) or (n^*), when starting from i completed steps. The TCR triggering probability is expressed as $\mathbb{P}_i^0$ if CD8 is unbound when TCR associates with the ligand, and $\mathbb{P}_i^*$ if CD8 is bound. The law of total probability yields the following system of recurrence relations:

$$\begin{aligned} \mathbb{P}_0^0 &= \frac{n\lambda}{n\lambda + \lambda_{-1} + \lambda_2}\mathbb{P}_1^0 + \frac{\lambda_2}{n\lambda + \lambda_{-1} + \lambda_2}\mathbb{P}_0^* \,, \\ \mathbb{P}_{i-1}^0 &= \mathbb{P}_a^0\mathbb{P}_i^0 + \mathbb{P}_b^0\mathbb{P}_{i-2}^0 + \mathbb{P}_c^0\mathbb{P}_{i-1}^* \quad \text{for} \quad i = 2\ldots n-1 \end{aligned} \tag{8}$$

for the chain with CD8 unbound, and

$$\begin{aligned} \mathbb{P}_0^* &= \frac{n\lambda^*}{n\lambda^* + \lambda_{-4} + \lambda_{-2}}\mathbb{P}_1^* + \frac{\lambda_{-2}}{n\lambda^* + \lambda_{-4} + \lambda_{-2}}\mathbb{P}_0^0 \,, \\ \mathbb{P}_{i-1}^* &= \mathbb{P}_a^*\mathbb{P}_i^* + \mathbb{P}_b^*\mathbb{P}_{i-2}^* + \mathbb{P}_c^*\mathbb{P}_{i-1}^0 \quad \text{for} \quad i = 2\ldots n-1 \end{aligned} \tag{9}$$

for the chain with CD8 bound. The boundary conditions are $\mathbb{P}_n = \mathbb{P}_n^* = 1$ since the probability of attaining the final state is 1 if starting from that state.

Finally, introducing the scaled parameters:

$$\alpha = \frac{\lambda_{-1}}{\lambda} \,; \quad \delta = \frac{\lambda_{-2}}{\lambda} \,; \quad \theta = \frac{\psi}{\lambda} \,; \quad \theta^* = \frac{\psi^*}{\lambda} \,, \tag{10}$$

we can write eqn (1) in dimensionless form:

$$w = \frac{W}{K_1 m_T \lambda} = \alpha \left(\frac{r}{1 + x + r + xr/\gamma_{\text{kin}}}\mathbb{P}_0^0 + \frac{xr\gamma_{\text{off}}}{\gamma_{\text{kin}}(1 + x + r) + xr}\mathbb{P}_0^* \right) . \tag{11}$$

The scaled TCR triggering rate w depends on the dimensionless parameters listed in Table 1; additional notation is as in previous work and summarised in Appendix A.

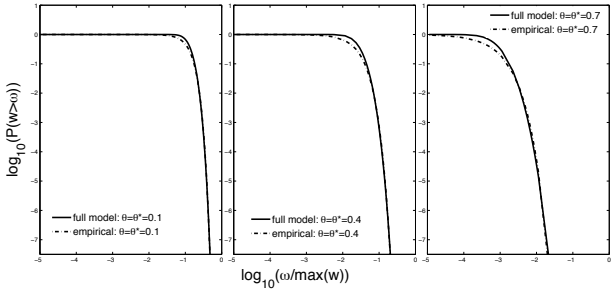

Fig. 3 Analysis of degeneracy Empirical approximation, eqn (12), compared with the probability $\mathbb{P}(w > \omega)$ for different values of the ITAM de-phosphorylation rate $\theta = \theta^* = 0.1$, $\theta = \theta^* = 0.4$, and $\theta = \theta^* = 0.7$. Parameter values: $n = 100$, $\delta = 300$, $\gamma_{\text{kin}} = 0.1$, $\gamma_{\text{off}} = 0.5$, $\gamma_{\text{R}} = 1$, $\kappa = 5.5$, $m_T = 10$, $r_T = 10$, and $x_T = 100$; for the log-normal distribution characterising the TCR/pMHCI dwell-time: $\mu = 2$ and $\sigma = 0.1$.

2.2 Characterisation of TCR degeneracy

From a probabilistic point of view, TCR degeneracy can be treated in terms of the probability that the TCR triggering rate w_{ij} exceeds a given value ω, where w_{ij} denotes the rate at which a pMHCI molecule of species i triggers TCR molecules of clonotype j. The quantity of interest is therefore $\mathbb{P}(w_{ij} > \omega)$, which we regard as a function of ω, for a fixed clonotype, ranging over the population of pMHCI ligands. The graph of this function ($\mathbb{P}(w_{ij} > \omega)$ in dependence of ω), called the "activation curve," is a visual representation of the degeneracy of the TCR clonotype at hand.

It has previously been established how $\mathbb{P}(w_{ij} > \omega)$ can be calculated as a function of ω by combining three key ingredients: (i) the kinetics; (ii) the triggering probability; and (iii) a distribution for the TCR/pMHCI dissociation rate[8,31,33,34]. Appendix B and Fig. 10 give an outline of the calculation, which relates the function $\mathbb{P}(w_{ij} > \omega)$ to the model parameters listed in Table 1. To study how these parameters affect degeneracy, it is convenient to define a suitable (scalar) index of degeneracy that can be derived from the function $\mathbb{P}(w_{ij} > \omega)$. This can be done in two steps. First, we fit the following approximation:

$$\exp\{\mathbb{P}(w_{ij} > \omega)\} \approx \frac{\exp\{-\exp\{\varpi_1 + \varpi_2\omega\} - \exp\{-\exp\{\varpi_1\}\}\}}{1 - \exp\{-\exp\{\varpi_1\}\}} \,, \tag{12}$$

where w_{ij} is assumed to have been scaled so that $0 \leq w_{ij} \leq 1$ (this scaling is dependent on θ and θ^* since these parameters affect the largest triggering rate that is physically attainable). Least-squares fitting the above formula to the $\mathbb{P}(w_{ij} > \omega)$ effectively amounts to a data-

Table 1 Parameters

m_T	scaled total pMHCI density
x_T	scaled total CD8 density
r_T	scaled total TCR density
α	scaled TCR/pMHCI off-rate without CD8 bound
δ	scaled pMHCI/CD8 off-rate with TCR bound
κ	ratio of dissociation constants K_1 and K_3
γ_{off}	scaled CD8 effect on TCR/pMHCI off-rate
γ_{kin}	scaled CD8 affinity effect
γ_{R}	scaled CD8 effect on ITAM phosphorylation
θ	scaled rate of ITAM de-phosphorylation without CD8 bound
θ^*	scaled rate of ITAM de-phosphorylation with CD8 bound

reduction step, in which the parameters listed in Table 1 are mapped to just two purely empirical parameters ϖ_1 and ϖ_2; the agreement is excellent, as shown in Fig. 3a. (This map is the composite of two maps: one is from the model parameters to the activation curve, the other is from this curve to the empirical parameters ϖ_1 and ϖ_2; overall then the original parameters are mapped to the pair (ϖ_1, ϖ_2).) The second step is to take the ratio ϖ_1/ϖ_2 to serve as an index of degeneracy. Examples of $\mathbb{P}(w_{ij} > \omega)$-curves and the corresponding values of ϖ_1/ϖ_2 are shown in Fig. 3b.

3 Results and discussion

We first consider the case when the co-receptor does not engage with the TCR/pMHCI complex, the "CD8-null case," followed by the general case.

3.1 The CD8-null case

When the co-receptor is absent or unable to engage the MHCI molecule (as is the case with certain MHC mutants) analytical expressions are available for the triggering probability (eqn (37) in Appendix C) as well as for the mean and variance of the triggering time T. As shown in Appendix C, the average waiting time for completion of all ITAM phosphorylations satisfies

$$\lambda \mathrm{E}(T) = \begin{cases} \dfrac{1}{n(1-\theta)}\left(n + \dfrac{\theta}{\theta-1}\left(\theta^n - 1\right)\right) & \text{if } \theta \neq 1; \\ \dfrac{n+1}{2} & \text{if } \theta = 1 \end{cases} \tag{13}$$

while the scaled variance is as follows when $\theta \neq 1$:

$$\lambda^2 \mathrm{Var}(T) = \frac{n(2\varsigma-1)(1+4\varsigma\theta^n)}{n^2(1+\theta)^2(1-2\varsigma)^4} + \frac{\varsigma(\theta^n-1)(4+\varsigma(\theta^n-3))}{n^2(1+\theta)^2(1-2\varsigma)^4} \tag{14}$$

where $\varsigma = 1/(1+\theta)$, and

$$\lambda^2 \mathrm{Var}(T) = \frac{1+2n+2n^2+n^3}{6n^2} \tag{15}$$

if $\theta = 1$. These results are represented in Figs 4a,b, showing that it takes longer to attain full phosphorylation when more phosphatase activity comes into play. This favours ligands with slower TCR/pMHCI dissociation rates; as shown in Fig. 4c, the dissociation rate associated with the optimal ligand increases with θ, the optimal ligands being approximately those with $\lambda_{-1} = 1/\mathrm{E}(T)$. Since such ligands occur less frequently, the effect of increasing θ is to make strong agonists rarer. It is apparent that expressing more PTPs, or in any event, allowing a higher activity of PTPs in the vicinity of the CD3, makes the TCR more selective. At the same time, the actual TCR triggering rate achieved at this optimum decreases with θ, as shown in the inset of Fig. 4d: enhanced PTP activity also makes pMHCI ligands less potent (unless the T-cell lowers its *cellular* activation threshold[4] along with increased PTP activity; such coordinated adjustment is not inconceivable).

Counteracting the effect of this increased selectivity is the effect of the PTPs on the variance, which also increases with θ, as shown in Fig. 4b. The effect of this increased variance is to enhance the triggering probability, as is made explicit by the following approximation:

$$\ln \mathbb{P}_0^0 \approx -\lambda_{-1}\mathrm{E}(T) + \ln\left\{1 + \tfrac{1}{2}\lambda_{-1}^2 \mathrm{Var}(T)\right\}\ ; \tag{16}$$

this result is derived in Appendix C.

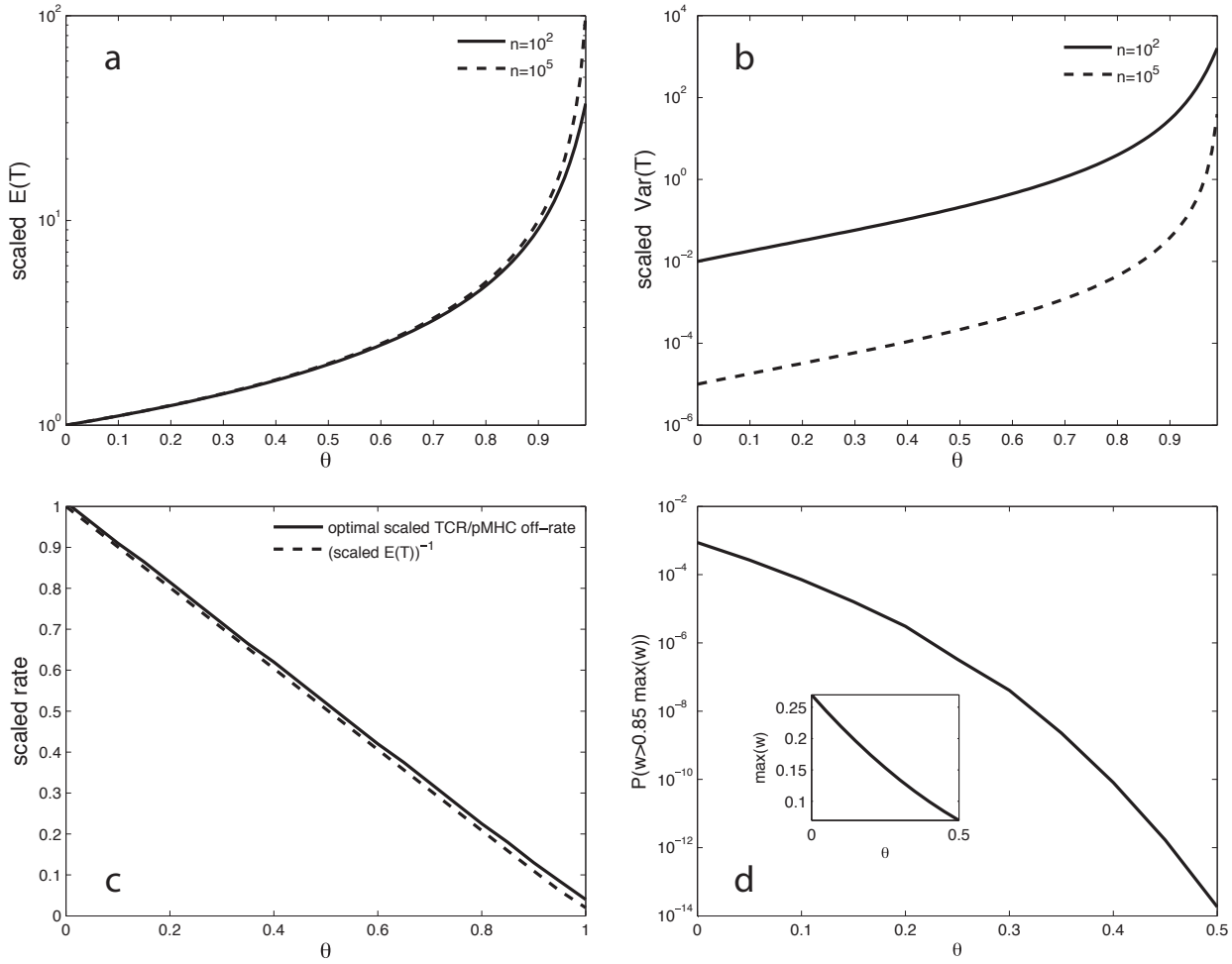

Fig. 4 The effect of PTPs in the CD8-null case (a), (b) Scaled $\mathrm{E}(T)$ and $\mathrm{Var}(T)$ as functions of the scaled ITAM de-phosphorylation rate θ. (c) For each value of the maximum possible triggering rate $\max(w)$, the corresponding optimal scaled TCR/pMHCI off-rate is shown as a function of θ (solid line). This quantity is compared to the reciprocal of the scaled mean triggering time $\mathrm{E}(T)$ (dashed line). (d) Statistical survivor function $\mathbb{P}(w > 0.85\max(w))$ for nearly optimal ligands as a function of θ. Here, the nearly optimal ligands are chosen such that their TCR triggering rate equals $0.85\max(w)$. The inset graph shows the dependence of $\max(w)$ on θ. Parameter values are as follows: $n = 100$, $m_T = 10$, $r_T = 10$ and for the TCR/pMHCI dwell-time log-normal distribution: $\mu = 1$ and $\sigma = 0.15$.

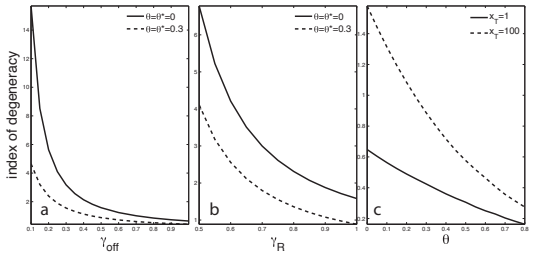

Fig. 5 Effects mediated by the co-receptor CD8 The effect of $\gamma_{\text{off}}, \gamma_{\text{R}}$, and x_T on the index of degeneracy (ϖ_1/ϖ_2) in the absence of ITAM de-phosphorylations (when $\theta = \theta^* = 0$) and in their presence (when $\theta = \theta^* = 0.3$). Parameter values are as follows: $n = 100$, $\delta = 300$, $\gamma_{\text{kin}} = 0.1$, $\gamma_{\text{off}} = 0.5$, $\gamma_{\text{R}} = 1$, $\kappa = 5.5$, $m_T = 10$, $r_T = 10$, $x_T = 100$; for the log-normal distribution characterising the TCR/pMHCI dwell-time: $\mu = 2$ and $\sigma = 0.1$.

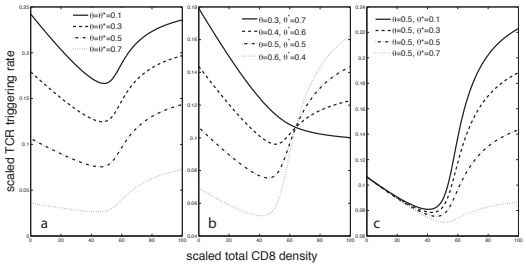

Fig. 6 Co-receptor-and PTK/PTPs balance cooperating in modulating the rate of TCR triggering Scaled functional sensitivity w as a function of the total scaled CD8 density x_T for different values of the ITAM de-phosphorylation rates with CD8 bound (θ) and without CD8 bound (θ^*). The pMHCI ligand has scaled dissociation rate $\alpha = 1$. Parameter values are as follows: $n = 100$, $\delta = 300$, $\gamma_{\text{kin}} = 0.1$, $\gamma_{\text{off}} = 0.5$, $\kappa = 5.5$, $\gamma_{\text{R}} = 1$, $m_T = 10$, and $r_T = 10$.

3.2 General model including the co-receptor CD8

The analysis is somewhat more complicated when the co-receptor comes into play.

3.2.1 Mean triggering time with involvement of the co-receptor CD8. In the case where the co-receptor can engage the TCR/pMHCI complex, we were unable to find an explicit formula for the mean triggering time $\mathrm{E}(T)$, except for the special case where $\theta = \gamma_R\theta^*$. It is not clear whether this is the case that prevails in the real biological system since the modulatory interactions between the co-receptor CD8 and PTPs are as yet poorly understood.

In the case $\theta = \gamma_R\theta^*$, we can calculate the expected number of jumps to reach the state where all ITAMs are fully phosphorylated. Let $\mathrm{E}(T)$ and $\mathrm{E}(T^*)$ denote the mean triggering times to reach the state of TCR triggering for the chains with CD8 unbound or bound when starting at the state of TCR/pMHCI docking. We then have the following equations for their weighted average of $\mathrm{E}(T)$ and $\mathrm{E}(T^*)$:

$$\frac{1}{1+\gamma_{\text{kin}}x/\gamma_R}\lambda\mathrm{E}(T)+\frac{\gamma_{\text{kin}}x/\gamma_R}{1+\gamma_{\text{kin}}x/\gamma_R}\lambda\mathrm{E}(T^*)= \frac{1+\gamma_{\text{kin}}x}{1+\gamma_{\text{kin}}x/\gamma_R}\frac{1}{n(1-\theta)}\left(n+\frac{\theta}{\theta-1}\left(\theta^n-1\right)\right), \quad (17)$$

if $\theta \neq 1$, and

$$\frac{1}{1+\gamma_{\text{kin}}x/\gamma_R}\lambda\mathrm{E}(T)+\frac{\gamma_{\text{kin}}x/\gamma_R}{1+\gamma_{\text{kin}}x/\gamma_R}\lambda\mathrm{E}(T^*)=\frac{n+1}{2}, \quad (18)$$

if $\theta = 1$. These results are derived in Appendix D.

3.2.2 Combined effects of CD8 and the PTK/PTP balance. With CD8 having no direct effect on PTP activity ($\theta = \theta^*$), the effects of CD8 and the PTK/PTP balance combine more or less independently, as shown in Fig. 5. CD8 stabilises the TCR/pMHCI interaction[35], which lengthens the mean duration of a receptor-ligand docking. This effect is expressed by the coefficient $\gamma_{\text{off}} \in [0,1]$, where $\lambda_{-4} = \gamma_{\text{off}}\lambda_{-1}$. Decreasing this coefficient has the effect of strengthening weak agonists and as these tend to be more numerous, the TCR becomes more degenerate, as shown in Fig. 5a, which also shows that increasing the activity of PTPs has the effect of reducing degeneracy more or less independently of γ_{off}.

The co-receptor CD8 also expedites the rate of ligand phosphorylation[14], which is expressed by the coefficient $\gamma_{\text{R}} \in [0,1]$, as shown in eqn (32). Again this allows weaker agonists to become more potent since completion of the ITAM phosphorylation sequence becomes more likely to occur even during short TCR/pMHCI docking events. The effect on TCR degeneracy is very similar as that of the kinetic effect, as shown in Fig. 5b, and again increasing PTP activity depresses degeneracy acting in a more or less additive (*i.e.* independent) fashion.

The decrease of degeneracy with the relative PTP activity (θ) is shown in Fig. 5c. Increasing the co-receptor density (x_T) increases degeneracy. Thus it appears that, within certain limits, the T-cell can adjust one of the two (CD8 or PTP) to compensate for the effect on degeneracy of the other factor.

3.2.3 Cross-talk between co-receptor and PTK/PTP balance. In the case $\theta \neq \theta^*$, the PTK/PTP balance shifts when the CD8 engages. It is not clear whether engagement of CD8 would favour PTKs or

PTPs: on the one hand, the co-receptor CD8 is believed to mediate the recruitment of TCR molecules to lipid rafts[36], which exclude PTPs such as CD45 and which may be privileged sites for TCR signalling[37]. This effect implies $\theta > \theta^*$, in the present notation. On the other hand, activation of Lck via TCR-agonist pMHCI ligation may be followed by this active Lck-CD8 complex finding and activating PTPs (like SHP-1), in analogy to the mechanism proposed by Hoerter et al.[38]. This would imply $\theta < \theta^*$. Given this uncertainty, we regard both cases as theoretical possibilities. A range of values of θ and θ^* is considered in Fig. 6: here CD8 exercises a modulatory effect, represented by the parameter $\gamma_{\rm kin}$, such that the TCR triggering rate is lowest at intermediate levels of CD8 and higher when CD8 is either below or above this intermediate value (as shown in eqn (31), $\gamma_{\rm kin}$ represents the effect on TCR/pMHCI kinetics; there is a second mode of action represented by $\gamma_{\rm R}$ but this parameter has been set to the "no-effect" value 1; cf. eqn (32)).

Fig. 6a shows how PTP activity depresses the TCR triggering rate more or less uniformly regardless of the CD8 levels when $\theta = \theta^*$. By contrast, Fig. 6b shows the high-CD8 effect is partially obscured when $\theta^* > \theta$ or, conversely, how triggering receives an additional boost when $\theta^* < \theta$. Keeping θ constant but varying θ^*, the T-cell can modulate the effect associated with high CD8 levels independently of the effect associated with low CD8 levels, as illustrated in Fig. 6c.

We have previously shown that, by varying CD8 levels, a T-cell can enhance the TCR triggering rate for one ligand while decreasing it for another[14,31]. This differential tuning effect, called "ligand focusing," allows the T-cell to change the relative ordering of potency among a series of ligands. The present results indicate that the T-cell can, in addition, adjust the magnitude of this reordering by adjusting the PTK/PTP balance.

3.3 Comparison to experimental data

In the setting of our theory, the TCR triggering rate is the key quantity corresponding to our intuitive concept of the strength or quality of the TCR/pMHCI interaction. Although it might be possible to measure this rate directly, in practice a different quantity is used to express agonist strength, which is the $p\mathrm{EC}_{50}$ obtained from a peptide titration assay. Here $p\mathrm{EC}_{50} = -\log_{10}\mathrm{EC}_{50}$, where EC_{50} stands for the concentration at which the effect (cellular response) is evoked in 50% of the subjects (T-cells). Under suitable assumptions, the TCR triggering rate can be taken to be proportional to the $p\mathrm{EC}_{50}$-value[7]; the constant of proportionality is unknown, but

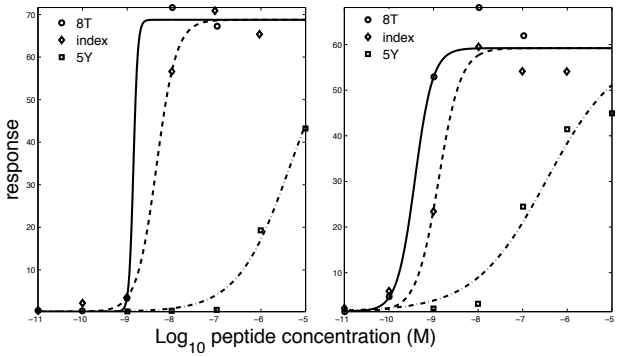

Fig. 7 Functional sensitivity assays Data originally obtained by Laugel et al.[39] from peptide titration experiments in which a T-cell response (CD107a up-regulation, expressed in arbitrary units) is measured upon interaction with APCs that were incubated with ligand peptide at various concentrations. The curves are the result of non-linear least-squares fitting the expression $y = y_0 + \Delta y / \left(1 + 10^{\varkappa(p\mathrm{EC}_{50} - pC)}\right)$, where y_0, Δy, and $\varkappa$ are nuisance parameters, $pC = -\log_{10}[\mathrm{peptide}]$ and $p\mathrm{EC}_{50}$ is the key parameter describing the midpoint location of the dose-response curve. The ligands are the index peptide ILAKFLHWL (diamonds), the variant peptide ILAKFLHTL (denoted as 8T; circles), and the variant peptide ILAKYLHWL (denited as 5Y; squares). Left: data obtained with APCs expressing the mutant MHC molecules which cannot engage the co-receptor CD8 (CD8-null); right: data obtained with the wild-type (WT) MHC molecule.

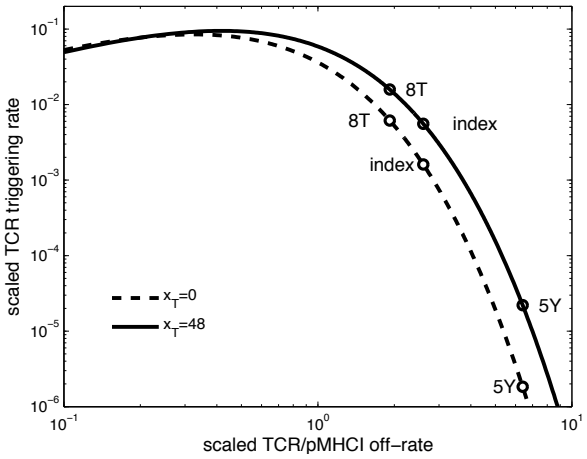

Fig. 8 Comparison to data The solid line represents the wild-type MHCI/CD8 condition with $x_T = 10$ and the dashed line represents the CD8-null case (simulated as $x_T = 0$). Parameter values used in the simulations: $n = 100$, $\delta = 300$, $\gamma_{\rm kin} = 0.1$, $\gamma_{\rm off} = 0.7$, $\gamma_{\rm R} = 1$, $\kappa = 2$, $m_T = 10$, $r_T = 10$, $\theta = \theta^* = 0.7$. The TCR/pMHCI off-rates have been scaled relative to $\lambda = 0.05\ s^{-1}$, resulting in $\alpha = 2.6$ for the index peptide, $\alpha = 1.92$ for variant 8T and $\alpha = 6.4$ for variant 5Y.

fortunately it cancels when we consider differences between ligands. In practice, a reference ligand is chosen and the difference between the $p\mathrm{EC}_{50}$-value of the peptide at hand and that of the reference serves as a measure of relative strength. The reference peptide is usually the index peptide, which is the agonist via which the clone was originally identified and isolated; it is by no means obligatory for the index peptide to be the best known agonist for the clone[7,39].

Examples of such data are shown in Fig. 7 for a T-cell clone that recognises a peptide derived from the catalytic subunit of the tumour-associated antigen human telomerase reverse transcriptase[39]; the index peptide as well as two variants called 8T and 5Y were titrated in these studies. These experiments were performed both with wild-type (WT) MHCI molecules as well as with mutant MHCI molecules that cannot associate with the co-receptor CD8, thus providing an experimental counterpart to the CD8-null case discussed in Section 3.1. For the WT interaction, the following data are found:

$$p\mathrm{EC}_{50}^{8\mathrm{T}} - p\mathrm{EC}_{50}^{\mathrm{index}} = +0.532 \qquad (19)$$

$$p\mathrm{EC}_{50}^{5\mathrm{Y}} - p\mathrm{EC}_{50}^{\mathrm{index}} = -2.426 \qquad (20)$$

which indicates that the functional sensitivity of this clone to the 8T variant is over 3-fold higher than to the index peptide, whereas the 5Y variant is ∼266-fold weaker than the index. For the CD8-null interaction, we find:

$$p\mathrm{EC}_{50}^{8\mathrm{T,\ CD8\text{-}null}} - p\mathrm{EC}_{50}^{\mathrm{index,\ CD8\text{-}null}} = +0.519 \qquad (21)$$

$$p\mathrm{EC}_{50}^{5\mathrm{Y,\ CD8\text{-}null}} - p\mathrm{EC}_{50}^{\mathrm{index,\ CD8\text{-}null}} = -2.996 \qquad (22)$$

indicating that now the 8T variant is ∼3-fold stronger than the index and the 5Y variant is about ∼1000-fold weaker than the index, indicating that the weakest ligand shows the strongest dependence on the presence of the co-receptor. Finally, the index interaction itself is ∼3-fold weaker in the CD8-null case:

$$p\mathrm{EC}_{50}^{\mathrm{index,\ CD8\text{-}null}} - p\mathrm{EC}_{50}^{\mathrm{index}} = -0.545\,. \qquad (23)$$

Although we cannot compare functional sensitivity to the TCR triggering rate directly, we can investigate whether the model can reproduce these x-fold differences. A useful constraint is that we also know the TCR/pMHCI dissociation rates for the WT interaction: 0.13 s^{-1} for the index peptide; 0.095 s^{-1} for 8T; and 0.32 s^{-1} for 5Y[4]. Such simulations are shown in Fig. 8: logarithmic distances between ligands and their shifts in response to the CD8-null mutation are in broad agreement with the data.

Now consider what happens to the functional sensitivities for these ligands when the phosphatases are taken out of play: this scenario is shown in Fig. 9. In the presence of CD8 at sufficiently high densities, the TCR triggering rates are now within an order of magnitude of one another—a dramatic shift from the previous situation.

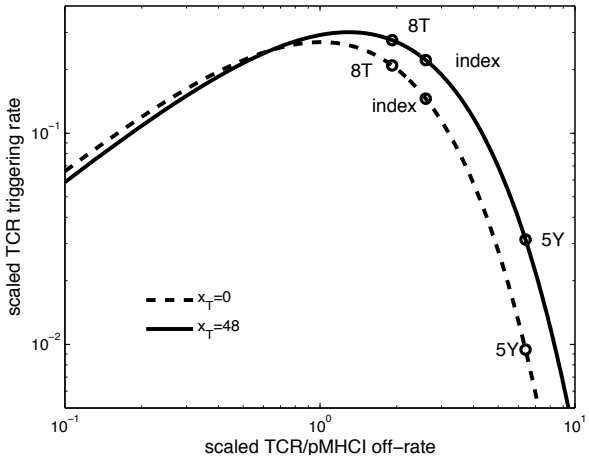

Fig. 9 Predicted shifts in functional sensitivity when phosphatase activity is abrogated Curves are for the same parameters values as in the previous figure, but with $\theta = \theta^* = 0$, *i.e.*, PTP activity is suppressed.

The physiological analogue of this situation is a privileged section within the T-cell:APC contact area. It has been proposed that CD45, a major PTP, is excluded from the area where TCR and pMHCI molecules congregate due to steric/thermodynamic effects, as TCR and pMHCI require a much closer apposition of the membranes of the participating cells than does CD45, which has a bulky extracellular domain[26,40]. Such exclusion of phosphatases from privileged domains within the T-cell:APC contact area, which has also been demonstrated for CD148[27] and SHP-1[28], underpins the "kinetic-segregation" model of T-cell activation which postulates that removal of PTPs is key to a shift in the PTK/PTP balance and hence in the modulation of TCR signalling[41].

The shift shown in Fig. 9 suggests a novel mechanism for the T-cell to gauge the quality of a ligand. A well-known phenomenon in T-cell biology is the "avidity effect," whereby a weaker agonist presented on a greater number of copies of the MHC molecule is equally potent as a strong agonist presented at lower densities (in fact, this is the effect exploited in the peptide titration curves shown in Fig. 8). In the notation of the present model, if m_j is the density of MHCI molecules presenting the ligand of species j, then $m_j w_{ij}$ is the signal a T-cell of clonotype i will register. Clearly, a decrease in w_{ij} can be compensated by an increase in m_j.

Now as the PTK/PTP-balance gradually shifts in

favour of PTKs as the T-cell:APC contact area matures[42], a weaker ligand profits more than a stronger one would—in other words, the time course of the TCR triggering rate over the lifetime of the T-cell:APC conjugation event provides the T-cell with information about the intrinsic quality of the ligand. Moreover, this is information which the T-cell in principle is able to decode, since it controls the PTK/PTP-balance. Much more than just a generic "brake" to keep signalling within a working range[43], PTPs can in fact help naive repertoire T-cells decide on their suitability for clonal expansion and differentiation into effector cells. This is a critical decision which an ideal system would take before committing massive resources to any particular clonotype.

4 Conclusions

Analysis of the TCR/pMHCI kinetics and stochastic dynamics of activation suggests that the co-receptor CD8 and the PTK/PTP balance, acting in concert, allow the T-cell to adjust the overall degeneracy of its ligand recognition and simultaneously fine-tune its functional sensitivity to specific salient peptide epitopes. Manipulation of these quantities in experiments or in immunotherapy holds great promise in increasing the efficacy of T-cells against pathogens and cancer, and in depressing their responsiveness in autoimmune disorders. The present model could provide a quantitative tool for the rational design of such interventions.

Acknowledgement BSz was supported by the Biotechnology and Biological Sciences Research Council (grant BB/H001085/1). Two anonymous referees provided helpful comments which greatly improved the presentation of the manuscript.

A TCR/pMHCI/CD8 kinetics

Our notation agrees with previous work[31]; the variables are listed in Table 2 and parameters in Table 1. The pMHCI, CD8, and TCR densities are subject to conservation laws:

$$M_T = M + M_R + M_X + M_{XR}\,; \tag{24}$$
$$X_T = X + M_X + M_{XR}\,; \tag{25}$$
$$R_T = R + M_R + M_{XR}\,. \tag{26}$$

Pseudo-unimolecular association rates λ_1–λ_4 are defined as follows (cf. Fig. 2):

$$\lambda_1 = \Lambda_1 R\,; \quad \lambda_2 = \Lambda_2 X\,; \quad \lambda_3 = \Lambda_3 X\,; \quad \lambda_4 = \Lambda_4 R\,. \tag{27}$$

Dissociation constants are defined as follows:

$$K_1 = \frac{\lambda_{-1}}{\lambda_1} R\,; \quad K_2 = \frac{\lambda_{-2}}{\lambda_2} X\,;$$
$$K_3 = \frac{\lambda_{-3}}{\lambda_3} X\,; \quad K_4 = \frac{\lambda_{-4}}{\lambda_4} R\,. \tag{28}$$

The principle of detailed balance states that at equilibrium the forward rate of each reaction step is equal to the reverse rate of that step:

$$\lambda_{-1} M_R = \lambda_1 M\,; \quad \lambda_{-2} M_{XR} = \lambda_2 M_R\,;$$
$$\lambda_{-3} M_X = \lambda_3 M\,; \quad \lambda_{-4} M_{XR} = \lambda_4 M_X\,, \tag{29}$$

whence $K_1 K_2 = K_3 K_4$. Combining this with eqns (24)–(26) and (28), we have:

$$M_R = M_T \frac{R}{K_1 + R + X K_1/K_3 + RX/K_2}\,;$$
$$M_X = M_T \frac{X}{K_3 + X + R K_3/K_1 + RX/K_4}\,;$$
$$M_{XR} = M_T \frac{XR}{K_1 K_2 + R K_2 + X K_4 + RX}\,. \tag{30}$$

The modulatory functions of the co-receptor CD8 can be represented in terms of dimensionless coefficients which we denote as a γ with an appropriate subscript: (i) enhanced TCR/pMHCI on-rate: $\Lambda_4 = \gamma_{\rm on}\Lambda_1$ where $\gamma_{\rm on} \geq 1$; (ii) reduced TCR/pMHCI off-rate: $\lambda_{-4} = \gamma_{\rm off}\lambda_{-1}$ where $0 < \gamma_{\rm off} \leq 1$; (iii) increased ITAM phosphorylation rate:

$$\lambda^* = \lambda/\gamma_{\rm R} \tag{31}$$

where $\gamma_{\rm R} \leq 1$. The combined co-receptor effect on the on-rate and off-rate is expressed as follows:

$$\gamma_{\rm kin} = \frac{\gamma_{\rm off}}{\gamma_{\rm on}} = \frac{K_4}{K_1} = \frac{K_2}{K_3}, \tag{32}$$

where $0 < \gamma_{\rm kin} \leq 1$. In terms of the modulatory coefficients we have:

$$M_R = M_T \frac{R/K_1}{1 + R/K_1 + X/K_3 + RX/(K_1 K_3 \gamma_{\rm kin})}\,;$$
$$M_X = M_T \frac{X/K_3}{1 + R/K_1 + X/K_3 + RX/(K_1 K_3 \gamma_{\rm kin})}\,;$$
$$M_{XR} = M_T \frac{RX/(K_1 K_3)}{\gamma_{\rm kin}(1 + X/K_3 + R/K_1) + RX/(K_1 K_3)}\,.$$

The system is rendered dimensionless in terms of the following quantities:

$$x = \frac{X}{K_3}\,; \quad r = \frac{R}{K_1}\,; \quad x_T = \frac{X_T}{K_3}\,;$$
$$r_T = \frac{R_T}{K_1}\,, \quad \kappa = \frac{K_1}{K_3}\,; \quad m_T = \frac{M_T}{K_1}\,, \tag{33}$$

Table 2 Variables

M	free pMHCI density
M_R	TCR/pMHCI density without CD8 bound
M_X	pMHCI/CD8 density without TCR bound
M_{XR}	TCR/pMHCI/CD8 density
X	free CD8 density
R	free TCR density
M_T	total pMHCI density
X_T	total CD8 density
R_T	total TCR density

which implies $M_T/K_3 = \kappa m_T$. On this scaling, we obtain the following nonlinear system of equations which can be numerically solved for x and r (using a fixed-point method), given the parameters $\gamma_{\rm kin}$, κ, r_T, m_T:

$$x_T = x + \kappa m_T \frac{x}{1+x+r+xr/\gamma_{\rm kin}} + \kappa m_T \frac{xr}{\gamma_{\rm kin}(1+x+r)+xr} ;$$

$$r_T = r + m_T \frac{r}{1+x+r+xr/\gamma_{\rm kin}} + m_T \frac{xr}{\gamma_{\rm kin}(1+x+r)+xr} .$$

B The TCR triggering rate distribution

TCR degeneracy can be represented mathematically in terms of the statistical distribution of w_{ij}[8,31,33,34], which denotes the rate at which a pMHCI molecule of species j triggers a TCR of clonotype i. To characterise this distribution, the key expression to derive is $\mathbb{P}(w_{ij} > \omega)$ for arbitrary ω. Let T_{ij} be the mean dwell time of the TCR/pMHCI interaction for TCR clonotype i and pMHCI species j (this means $T_{ij} = \lambda_{-1}^{-1} = (\alpha\lambda)^{-1}$). Arrhenius theory[44] posits $T_{ij} = T_0 \exp(\Delta U_{ij})$ where T_0 is the frequency factor and ΔU_{ij} is the dissociation energy barrier, expressed in Boltzmann units. This barrier can be regarded as the sum of a large number of atomic interactions at the TCR/pMHCI interface. If these combine additively, then ΔU_{ij} has a Gaussian distribution by the Central Limit Theorem[45]. We define a scaled version of this energy, as follows:

$$u_{ij} = \Delta U_{ij} - \ln\{\lambda^{-1}/T_0\} . \qquad (34)$$

We assume that this variate is Gaussian: $u_{ij} \sim \mathcal{N}(-\mu_i, \sigma_i^2)$, where $\mu_i > 0$ and σ_i are the location and specificity parameters. Hence, the scaled TCR/pMHCI off-rate α is log-normally distributed. The assumption

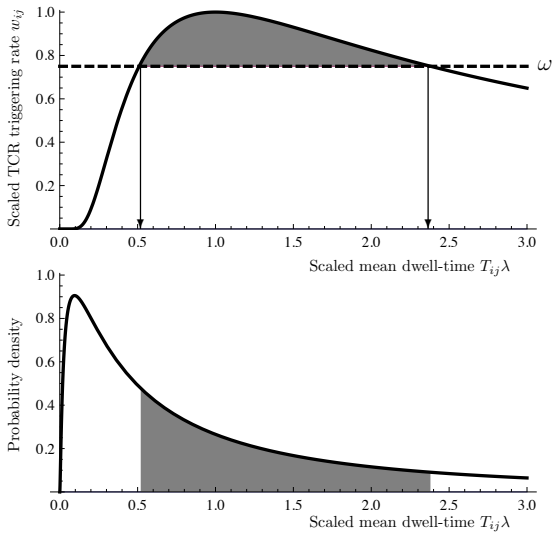

Fig. 10 Calculation of the TCR triggering rate distribution Top panel: dependence of the triggering rate w_{ij} on the mean interaction time T_{ij}. The condition $w_{ij} > \omega$, a key quantity for the TCR triggering rate distribution $\mathbb{P}(w_{ij} > \omega)$, corresponds to the TCR triggering rate exceeding the value ω (indicated by the horizontal dashed line). This corresponds to the portion marked in solid grey, and requires T_{ij} to lie between the two values of $T_{ij}\lambda$ that are indicated by arrows pointing to the abscissa. These values form the integration limits for the log-normal probability density function of T_{ij} (bottom panel) which is integrated between these limits to give $\mathbb{P}(w_{ij} > \omega)$, i.e. the probability of w_{ij} exceeding ω. The value for this probability obtained in this example is in fact unphysiologically high, for the sake of illustrating the principle.

that the mean is negative reflects the fact that the vast majority of pMHCI ligands are weak binders.

Now assume that we have w_{ij} as a function of T_{ij} (for instance eqn (35) below, this being a special case). The calculation of $\mathbb{P}(w_{ij} > \omega)$ then proceeds as explained graphically in Fig. 10.

In the special case when the co-receptor CD8 is absent, the kinetic regime is MHC-limited (see[4]), and ITAMs are phosphorylated but not de-phosphorylated ($\psi = \psi^* = 0$), we can calculate the probability $\mathbb{P}(w_{ij} > \omega)$. The TCR triggering rate is then given by

$$W_{ij} = M_T T_{ij} \exp\{-\lambda T_{ij}\} , \qquad (35)$$

which has a maximum where the mean dwell-time T_{ij} equals $1/\lambda$[46]. The scaling $w_{ij} = (M_T\lambda)^{-1} e W_{ij}$ yields the convenient restriction $0 \le w_{ij} \le 1$. The MHC-specific scaled triggering rate is related to the scaled en-

ergy barrier u_{ij} by

$$w_{ij} = \exp\{1 - u_{ij} - e^{-u_{ij}}\} . \quad (36)$$

The equation $w = \omega$ has two roots, which are

$$u_{-1}(w) = 1 + \mathscr{W}_{-1}(-w/e) - \ln w \quad \text{and}$$
$$u_0(w) = 1 + \mathscr{W}_0(-w/e) - \ln w ,$$

where $\mathscr{W}$ is the Lambert W-function[47] and $u_{-1}(w) < u_0(w)$. Hence, the probability that the functional sensitivity of TCR clonotype i for peptide ligand species j will exceed a set value ω is given by

$$\mathbb{P}(w_{ij} > \omega) = \mathbb{P}(u_{-1}(\omega) \le u_{ij} \le u_0(\omega))$$
$$= \frac{1}{2}\left(\operatorname{erf}\left(\frac{1+\mu_i+\mathscr{W}_0(-\omega/e)-\ln\omega}{\sqrt{2}\sigma_i}\right) - \operatorname{erf}\left(\frac{1+\mu_i+\mathscr{W}_{-1}(-\omega/e)-\ln\omega}{\sqrt{2}\sigma_i}\right)\right),$$

where erf is the error function and (μ_i, σ_i) are the parameters of the Gaussian assumed for the scaled energy barrier u_{ij}. The MHC-limited case corresponds most closely to the classic serial triggering scenario originally envisaged by Valitutti c.s.[15,16]. This is the kinetic regime[30] that immunologists often tacitly assume to be physiologically relevant[17].

C Explicit results for the CD8-null case

The triggering probability $\mathbb{P}_0^0$ for the CD8-null case is determined by the following system:

$$\mathbb{P}_n^0 = 1 ;$$
$$\mathbb{P}_{i-1}^0 = \mathbb{P}_a^0\mathbb{P}_i^0 + \mathbb{P}_b^0\mathbb{P}_{i-2}^0 \text{ for } 2 \le i \le n-1 ;$$
$$\mathbb{P}_1^0 = P_{11}\mathbb{P}_0^0 ,$$

where $\mathbb{P}_a^0$ and $\mathbb{P}_b^0$ are defined by eqns (2)–(5), and P_{11} is defined as follows:

$$P_{11} = \frac{n\lambda + \lambda_{-1}}{n\lambda} .$$

Then $\mathbb{P}_0^0$ has the form

$$\mathbb{P}_0^0 = \frac{(\mathbb{P}_a^0)^{n-1}}{A-B} , \quad (37)$$

where A and B are given by

$$A = (P_{11} - \mathbb{P}_b^0)(K_1U^{n-3} + L_1V^{n-3}) + \mathbb{P}_a^0\mathbb{P}_b^0P_{11}(K_2U^{n-3} + L_2V^{n-3}) ;$$
$$B = \mathbb{P}_a^0\mathbb{P}_b^0\Big[(P_{11} - \mathbb{P}_b^0)(K_1U^{n-4} + L_1V^{n-4}) + \mathbb{P}_a^0\mathbb{P}_b^0P_{11}(K_2U^{n-4} + L_2V^{n-4})\Big]$$

with

$$U = \frac{1+\sqrt{1-4\mathbb{P}_a^0\mathbb{P}_b^0}}{2} ; \quad V = \frac{1-\sqrt{1-4\mathbb{P}_a^0\mathbb{P}_b^0}}{2} ;$$
$$K_1 = \frac{1-V}{U-V} ; \quad L = 1 - K_1 ;$$
$$K_2 = -\frac{1}{U-V} , \quad L_2 = -K_2 .$$

The case $A = B$ is not physiologically relevant.

To calculate the expected triggering time and its variance, we borrow a result from Weesakul[48], who considered a random walk between reflecting and absorbing barrier. In our system, (0) is a reflecting barrier and (n) is an absorbing one. Weesakul[48] gives an explicit formula for the generating function associated with this random walk. Accordingly, we consider

$$\phi(\vartheta|u) = \sum_{k\ge 0} g(k|u)\vartheta^k,$$

where $g(k|u)$ is the probability of reaching the triggered state (n) in exactly k jumps starting from u, and the jumps may occur in both forward and backward directions. Given $\phi(\vartheta|u)$ we can calculate the expectation and variance of the triggering time, as follows. First, assume that triggering is achieved in exactly k steps, which happens with probability $g(k|u)$. The time required to reach the final time is a Gamma variate defined as follows:

$$Z_k = X_1 + X_2 + \cdots + X_k ,$$

where each of the random variables $X_1, \ldots, X_k$ independently follows an exponential distribution with mean $\xi = (n\lambda + n\psi)^{-1}$. Accordingly, $\mathrm{E}(Z_k) = k\xi$ and $\mathrm{E}(Z_k^2) = (k+k^2)\xi^2$. The first and second moments are

$$\mathrm{E}(Z) = \sum_{k\ge 0} g(k|u)E(Z_k) = \xi\sum_{k\ge 0} g(k|u)t = \xi\phi'(1|u)$$

and

$$\mathrm{E}(Z^2) = \sum_{k\ge 0} g(k|u)\mathrm{E}(Z_k^2)$$
$$= \xi^2\sum_{k\ge 0} g(k|u)(k^2+k) = \xi^2[\phi''(1|u) + 2\phi'(1|u)] ,$$

where the derivatives ϕ' and ϕ'' are with respect to ϑ. This yields the variance:

$$\mathrm{E}(Z^2) - \mathrm{E}(Z)^2 = \xi^2[\phi''(1) + 2\phi'(1) - (\phi'(1))^2] .$$

We set $\phi(\vartheta) = \phi(\vartheta|0)$. Using eqn (11) from Weesakul[48] for $\phi(\vartheta)$, we obtain eqns (13)–(15).

More generally, the sth moment is given by

$$\mathrm{E}(Z_k^s) = \xi^s k(k+1)\dots(k+s-1)$$

which allows us to write

$$\mathrm{E}(Z^s) = \sum_{k\geq 0} g(k|u)\mathrm{E}(Z_k^s) = \xi^s \sum_{k\geq 0} g(k|u)k(k+1)\dots(k+s-1)\,.$$

From the definition of the moment generating function $\phi(\vartheta|u)$ for the probabilities of absorption $g(k|u)$, we have

$$\mathrm{E}(Z^s) = \xi^s \frac{d^s}{d\vartheta^s}\left[L(\vartheta)\right]\Big|_{\vartheta=1}\,, \tag{38}$$

where $L(\vartheta) = \phi(\vartheta|u)\vartheta^{s-1}$. It can be shown that

$$\frac{d^s}{d\vartheta^s}\left[L(\vartheta)\right]\Big|_{\vartheta=1} = \frac{d^s}{d\vartheta^s}\left[\phi(\vartheta|u)\right]\Big|_{\vartheta=1} + \sum_{j=1}^{s-1}\frac{s!}{(s-j-1)!}\frac{d^j}{d\vartheta^j}\left[\phi(\vartheta|u)\right]\Big|_{\vartheta=1}\,.$$

To evaluate $\frac{d^j}{d\vartheta^j}\left[\phi(\vartheta|u)\right]\Big|_{\vartheta=1}$, we apply Weesakul's[48] formula for $\phi(\vartheta|u)$ with $m = 1/(1+\theta)$:

$$\phi(\vartheta|u) = \frac{\vartheta^u(1-m)^u\left[\lambda_1^{n-u+1} - \lambda_2^{n-u+1} - \vartheta m(\lambda_1^{n-u} - \lambda_2^{n-u})\right]}{\lambda_1^{n+1} - \lambda_2^{n+1} - \vartheta m(\lambda_1^n - \lambda_2^n)}\,, \tag{39}$$

where

$$\lambda_{1,2} = \frac{1}{2}\left(1 \pm \sqrt{1 - 4\vartheta^2 m(1-m)}\right)\,.$$

To derive eqn (16), let T denote the time for the CD3 complex to attain full phosphorylation and let $F_T(\tau) = \mathbb{P}(T \leq \tau)$ denote the cumulative distribution function. Then

$$\mathbb{P}_0^0 = \int_0^\infty \mathbb{P}(\text{triggering} \mid T = \tau) dF_T(\tau)\,,$$

where the probability in the integrand equals the probability of the TCR/pMHCI docking lasting for at least a time T. The TCR/pMHCI interaction time follows an exponential distribution with mean $1/\lambda_{-1}$. Hence

$$\mathbb{P}_0^0 = \int_0^\infty \exp\{-\lambda_{-1}\tau\} dF_T(\tau)\,.$$

We now apply the approximation $\mathrm{E}[f(T)] \approx f(\mathrm{E}(T)) + f''(\mathrm{E}(T))\mathrm{Var}(T)/2$, where f is an at least twice differentiable function; this formula is readily derived using a Taylor expansion and the definitions of the central moments[45]. This gives

$$\mathbb{P}_0^0 \approx \exp\{-\lambda_{-1}E(T)\}\left(1 + \tfrac{1}{2}\lambda_{-1}^2\mathrm{Var}(T)\right)\,, \tag{40}$$

which can be rewritten as eqn (16). In the limits $\theta \to 0$, $n \to \infty$, the variance $\mathrm{Var}(T)$ vanishes and hence the simple formula $\mathbb{P}_0^0 = \exp\{-\lambda_{-1}E(T)\}$ becomes exact.

D Explicit results for the case $\theta = \gamma_R\theta^*$

Assume $\lambda/\psi = \lambda^*/\psi^*$ and let ρ_i be the mean time to transit from state i to the final state n. Then we have the following recursive equations for the two chains:

$$\begin{aligned} &\rho_0 = \zeta + p\rho_1 + q\rho_0 + r\rho_0^*\,; \quad \rho_n = 0\,; \\ &\rho_i = \zeta + p\rho_{i+1} + q\rho_{i-1} + r\rho_i^* \;\text{ for }\; i = 1\dots n-1 \end{aligned} \tag{41}$$

in the case where CD8 is not bound, and

$$\begin{aligned} &\rho_0^* = \zeta^* + p^*\rho_1^* + q^*\rho_0^* + r^*\rho_0\,; \quad \rho_n^* = 0\,; \\ &\rho_i^* = \zeta^* + p^*\rho_{i+1}^* + q^*\rho_{i-1}^* + r^*\rho_i \;\text{ for }\; i = 1\dots n-1 \end{aligned} \tag{42}$$

in the case where CD8 is engaged. Here ζ is the mean time spent in state i, *i.e.*, $\zeta = 1/(n\lambda + n\psi + \lambda_2)$ for the chain without CD8 bound and $\zeta^* = 1/(n\lambda^* + n\psi^* + \lambda_{-2})$ for the chain with CD8 bound. The probabilities are $p = n\lambda/(n\lambda + n\psi + \lambda_2)$, $q = n\psi/(n\lambda + n\psi + \lambda_2)$, and $r = 1 - p - q$ for the chain without CD8 bound and $p^* = n\lambda^*/(n\lambda^* + n\psi^* + \lambda_{-2})$, $q^* = n\psi^*/(n\lambda^* + n\psi^* + \lambda_{-2})$ and $r^* = 1 - p^* - q^*$ for the chain with CD8 bound. Using these relations and multiplying eqn (41) by r^* and eqn (42) by r, we obtain

$$\begin{aligned} rr^*(\rho_i - \rho_i^*) &= \zeta r^* + pr^*(\rho_{i+1} - \rho_i) + qr^*(\rho_{i-1} - \rho_i)\,; \\ rr^*(\rho_i^* - \rho_i) &= \zeta^* r + p^* r(\rho_{i+1}^* - \rho_i^*) + q^* r(\rho_{i-1}^* - \rho_i^*)\,. \end{aligned}$$

In the case $\theta = \theta^*$ we have $p^*/p = q^*/q$ and therefore $p^* = \iota p$ and $q^* = \iota q$. Adding the previous equations we obtain:

$$\begin{aligned} 0 = {} & p(r^*\rho_{i+1} + \iota r\rho_{i+1}^*) - p(r^*\rho_i + \iota r\rho_i^*) + \\ & q(r^*\rho_{i-1} + \iota r\rho_{i-1}^*) - q(r^*\rho_i + \iota r\rho_i^*) + \zeta r^* + \zeta^* r\,. \end{aligned} \tag{43}$$

Let $\Pi_i = r^*\rho_i + \iota r\rho_i^*$ and $x_i = \Pi_{i-1} - \Pi_i$. Equation (43) can be rewritten as

$$x_{i+1} = \frac{q}{p}x_i + s\,, \;\text{ where }\; s = \frac{\zeta r^* + \zeta^* r}{p}\,.$$

The sequence $\{x_i\}_{i=1}^n$ defines a partial sum of a geometric series which is

$$x_n = \frac{1-(q/p)^n}{1-q/p}s\,, \tag{44}$$

which yields an analytical formula for

$$\Pi_0 = r^*\rho_0 + \imath r\rho_0^* = \Pi_n + x_1 + x_2 \ldots x_n\,.$$

Dividing both sides of eqn (44) by the weighted average $r^* + \imath r$ and noting that

$$r = \lambda_2\zeta \quad \text{and} \quad r^* = \lambda_{-2}\zeta^*\,,$$

we find

$$\frac{\lambda_{-2}}{\lambda_{-2}+\lambda_2/\gamma_R}\mathrm{E}(T) + \frac{\lambda_2/\gamma_R}{\lambda_{-2}+\lambda_2/\gamma_R}\mathrm{E}(T^*) = \frac{\lambda_{-2}+\lambda_2}{\lambda_{-2}+\lambda_2/\gamma_R}\cdot\frac{1}{n(\lambda-\psi)}\left(n + \frac{\psi}{\lambda-\psi}\left[\left(\frac{\psi}{\lambda}\right)^n - 1\right]\right)$$

whence we obtain eqn (17) which applies when $\lambda \neq \psi$. Equation (18) for the case $\lambda = \psi$ can be derived analogously.

References

1 G. P. Morris and P. M. Allen, *Nature Immunol.*, 2012, **13**, 121–128.
2 O. Acuto, V. D. Bartolo and F. Michel, *Nat. Rev. Immunol.*, 2008, **8**, 699–712.
3 P. D. Holler and D. M. Kranz, *Immunity*, 2003, **18**, 255–264.
4 H. A. van den Berg, K. Ladell, K. Miners, B. Laugel, S. Llewellyn-Lacey, M. Clement, D. K. Cole, E. Gostick, L. Wooldridge, A. K. Sewell, J. S. Bridgeman and D. A. Price, *Front. Immunol.*, 2013, **4**, a250.
5 H. S. Robins, P. V. Campregher, S. K. Srivastava, A. Wacher, C. J. Turtle, O. Kahsai, S. R. Riddell, E. H. Warren and C. S. Carlson, *Blood*, 2009, **114**, 4099–4107.
6 E. R. Stirk, C. Molina-París and H. A. van den Berg, *J. Theor. Biol.*, 2008, **255**, 237–249.
7 L. Wooldridge, J. Ekeruche-Makinde, H. A. van den Berg, A. Skowera, J. J. Miles, M. P. Tan, G. Dolton, M. Clement, S. Llewellyn-Lacey, D. A. Price, M. Peakman and A. K. Sewell, *J. Biol. Chem.*, 2012, **287**, 1168–1177.
8 H. A. van den Berg, D. A. Rand and N. J. Burroughs, *J. Theor. Biol.*, 2001, **209**, 465–486.
9 P. E. Love and S. M. Hayes, *Cold Spring Harb. Perspect. Biol.*, 2010, **2**, a002485.
10 D. K. Cole, B. Laugel, M. Clement, D. A. Price, L. Wooldridge and A. K. Sewell, *Immunology*, 2012, **137**, 139–148.
11 L. Wooldridge, B. Laugel, J. Ekeruche, M. Clement, H. A. van den Berg, D. A. Price and A. K. Sewell, *J. Immunol.*, 2010, **185**, 4625–4632.
12 J. H. Park, S. Adoro, P. J. Lucas, S. D. Sarafova, A. S. Alag, L. L. Doan, B. Erman, X. Liu, W. Ellmeier, R. Bosselut, L. Feigenbaum and A. Singer, *Nat. Immunol.*, 2007, **8**, 1049–1059.
13 M. N. Artyomov, M. Lis, S. Devadas, M. M. Davis and A. K. Chakraborty, *Proc. Natl. Acad. Sci. USA*, 2010, **107**, 16916–16921.
14 H. A. van den Berg, L. Wooldridge, B. Laugel and A. K. Sewell, *J. Theor. Biol.*, 2007, **249**, 395–408.
15 S. Valitutti, S. Müller, M. Cella, E. Padovan and A. Lanzavecchia, *Nature*, 1995, **375**, 148–151.
16 S. Valitutti and A. Lanzavecchia, *Immunol. Today*, 1997, **18**, 299–304.
17 A. M. Kalergis, N. Boucheron, M. A. Doucey, E. Palmieri, E. C. Goyarts, Z. Vegh, I. F. Luescher and S. G. Nathenson, *Nat. Immunol.*, 2001, **2**, 229–234.
18 J. D. Rabinowitz, C. Beeson, D. S. Lyons, M. M. Davis and H. M. McConnell, *Proc. Natl. Acad. Sci. USA*, 1996, **93**, 1401–1405.
19 S. Tian, R. Maile, E. J. Collins and J. A. Frelinger, *J. Immunol.*, 2007, **179**, 2952–2960.
20 S. M. Stanford, N. Rapini and N. Bottini, *Immunology*, 2012, **137**, 1–19.
21 I. Rhee and A. Veillette, *Nat. Immunol.*, 2012, **13**, 439–447.
22 T. Mustelin, K. M. Coggeshall and A. Altman, *Proc. Natl. Acad. Sci. USA*, 1989, **86**, 6302–6306.
23 E. Hui and R. D. Vale, *Nat. Struct. Mol. Biol.*, 2014, **21**, 133–142.
24 E. Vivier and B. Malissen, *Nat. Immunol.*, 2005, **6**, 17–21.
25 T. W. McKeithan, *Proc. Natl. Acad. Sci. USA*, 1995, **92**, 5042–5046.
26 O. Leupin, R. Zaru, T. Laroche, S. Müller and S. Valitutti, *Curr. Biol.*, 2000, **10**, 277–280.
27 J. Lin and A. Weiss, *J. Cell Biol.*, 2003, **162**, 673–682.
28 Y. M. Vyas, H. Maniar and B. Dupont, *J. Immunol.*, 2002, **168**, 3150–3154.
29 Y. D. Mahnke, T. M. Brodie, F. Sallusto, M. Roederer and E. Lugli, *Eur. J. Immunol.*, 2013, **43**, 2797–2809.
30 H. A. van den Berg, N. J. Burroughs and D. A. Rand, *Bull. Math. Biol.*, 2002, **64**, 781–808.
31 B. Szomolay, T. Williams, L. Wooldridge and H. A. van den Berg, *Front. Immunol.*, 2013, **4**, a329.
32 A. B. Bortz, M. H. Kalos and J. L. Lebowitz, *J. Comp. Phys.*, 1975, **17**, 10–18.
33 N. Zint, E. Baake and F. den Hollander, *J. Math. Biol.*, 2008, **57**, 841–861.
34 H. Mayer and A. Bovier, *J. Math. Biol.*, 2014, DOI:10.1007/s00285–014–0759–x.
35 L. Wooldridge, H. A. van den Berg, M. Glick, E. Gostick, B. Laugel, S. L. Hutchinson, A. Milicic, J. Brenchley, D. C. Douek, D. A. Price and A. K. Sewell, *J. Biol. Chem.*, 2005, **280**, 27491–27501.
36 A. Arcaro, C. Grégoire, T. R. Bakker, L. Baldi, M. Jordan, L. Goffin, N. Boucheron, F. Wurm, A. van der Merwe, B. Malissen and I. F. Luescher, *J. Exp. Med.*, 2001, **194**, 1485–1495.
37 A. K. Sewell, *Trends Immunol.*, 2002, **23**, 124.
38 J. A. H. Hoerter, J. Brzostek, M. N. Artyomov, S. M. Abel, J. Casas, V. Rybakin, J. Ampudia, C. Lotz, J. M. Connolly, A. K. Chakraborty, K. G. Gould and N. R. J. Gascoigne, *J. Exp. Med.*, 2013, **210**, 1807–1821.
39 B. Laugel, H. A. van den Berg, E. Gostick, D. K. Cole, L. Wooldridge, J. Boulter, A. Milicic, D. A. Price and A. K. Sewell, *J. Biol. Chem.*, 2007, **282**, 23799–23810.
40 K. Choudhuri, M. Parker, A. Milicic, D. K. Cole, M. Shaw, A. K. Sewell, G. Stewart-Jones, T. Dong, K. G. Gould and P. A. van der Merwe, *J. Biol. Chem.*, 2009, **284**, 26096–26105.
41 S. J. Davis and P. A. van der Merwe, *Immunol. Today*, 1996, **17**, 177–187.
42 S. Kumari, S. Vardhana, M. Cammer, S. Curado, L. Santos, M. P. Sheetz and M. L. Dustin, *Front. Immunol.*, 2012, **3**, a320.
43 R. Zamoyska, *Immunity*, 2007, **27**, 421–423.

44 N. G. van Kampen, *Stochastic Processes in Physics and Chemistry*, Elsevier, 2007.
45 L. J. Bain and M. Engelhardt, *Introduction to Probability and Mathematical Statistics*, Cengage Learning, 2000.
46 H. A. van den Berg and A. K. Sewell, *Mathematical Models and Immune Cell Biology*, Springer, 2011, pp. 47–73.
47 R. M. Corless, G. H. Gonnet, D. E. G. Hare, D. J. Jeffrey and D. E. Knuth, *Adv. Comput. Math.*, 1996, **5**, 329 – 359.
48 B. Weesakul, *Ann. Math. Statist.*, 1961, **32**, 765–769.